Pergamon

Int. J. Heat Mass Transfer. Vol. 37, No. 13, pp. 1935–1943, 1994

0017-9310/94 $7.00 + 0.00

0017-9310(94)E0033-Q

Morphological instability on Bénard–Marangoni convection during solidification: single-component system

MING-I CHAR and KO-TA CHIANG

Department of Applied Mathematics, National Chung Hsing University, Taichung, Taiwan 40227, Republic of China

(*Received* 12 *September* 1993)

Abstract—The critical conditions for the Bénard–Marangoni convective and morphological instabilities of a horizontal liquid layer of a single component, subject to a solidification process from below, are studied. The morphological effects, including the thickness and thermal conductivity of the solid layer and the capillary effect of the solid–liquid interface, have significant influences on the onset of instabilities at the marginal state. The analysis is based on the linear stability theory and the resulting eigenvalue equations are solved, using the shooting technique of Runge–Kutta–Gill's method of order four. The eigenvalue Rayleigh number, R, or Marangoni number, M, is evaluated. The numerical results indicate that the critical conditions decrease sensitively with the thickness ratio A for $0 < A < 1$ and approach fixed values for A becoming large. The effects of the capillarity at the solid–liquid interface and thermal conductivity in the solid layer tend to stabilize the system. The conducting ways of the latent heat act as dominant roles on determining the possible instability of the system.

INTRODUCTION

THE THEORY of the morphological stability of a solid–liquid interface during the solidification of a dilute binary alloy has been studied [1]. Morphological instability can be coupled with thermosolutal convective instabilities through the mutual interaction of thermal and solutal gradients, which in turn have a major effect on the interfacial growth, deformation and movement [2–6]. These studies show that a stationary or oscillatory mode may occur. Either thermosolutal convective or morphological instability can solely deform an initial planar interface into a nonplanar one. The pattern formation during the crystal growth, with or without thermosolutal effects, has been studied [7–9]. The onset of thermal or thermosolutal convective instabilities in a horizontal fluid layer has been studied [10, 11]. Davis *et al.* [12] consider the pattern selection of a horizontal liquid layer of a single-component, coupling Bénard convection and solidification.

In these analyses above, the upper boundary is either assumed rigid or located at infinity. For a horizontal liquid layer of finite thickness with its upper surface free, the variation of surface tension with the temperature is also one of the main factors for causing the convective instability, referred to as Marangoni instability [13, 14]. The combined effects of the thermal buoyancy and surface tension, known as Bénard–Marangoni instability, have been extensively studied [15–17].

The purpose of the present study is concerned with the morphological effects on the Bénard–Marangoni instability of a horizontal liquid layer of a single component with a finite thickness during the solidification.

MATHEMATICAL FORMULATION

A horizontal liquid layer of a single component is cooled from above and the freezing takes place in the lower part of the layer such that there exists a solid–liquid interface. The physical configuration is shown in Fig. 1. We assume that the fluid is incompressible and the fluid density variation based on the Boussinesq's approximation can be expressed as:

$$\rho = \rho_0[1-\alpha(T-T_0)], \tag{1}$$

where α is the coefficient of thermal expansion and ρ_0 is the density at the reference temperature T_0. The governing equations are [1–4]:

$$\nabla\cdot V = 0, \tag{2}$$

$$\frac{\partial V}{\partial t}+(V\cdot\nabla)V = -\frac{\nabla p}{\rho_0}-g\alpha(T-T_0)e_z+\nu\nabla^2 V, \tag{3}$$

$$\frac{\partial T}{\partial t}+(V\cdot\nabla)T = \kappa\nabla^2 T, \tag{4}$$

where $V=(u,v,w)$ is the fluid velocity and T is the temperature in the liquid layer, p is the pressure, ν is the kinematic viscosity and κ is the thermal diffusivity.

The boundary conditions of the solid–liquid interface, at $z=\eta(x,y,t)$, are that the tangential components of the fluid velocity vanish (i.e. no-slip condition):

NOMENCLATURE

a the wavenumber of the small disturbance
A thickness ratio, h_S/h_L
Bi Biot number, Hh_L/K_L
Bo Bond number, $\rho g h_L^2/\gamma$
C Crispation number, $\mu\kappa/\gamma h_L$
C_a capillarity number at solid–liquid interface, $T_M\Gamma/\Delta T_L h_L$
e_z unit vector in the z-direction
g gravitational acceleration
h_L, h_S thickness of liquid and solid plate
H heat transfer coefficient of the liquid layer
K thermal conductivity
L_v the latent heat of fusion per unit volume of solid
M Marangoni number, $\tau\Delta T h_L/\nu\kappa\rho$
p pressure
Pr Prandtl number, ν/κ
R Rayleigh number, $\alpha g\Delta T h_L^3/\nu\kappa$
S latent heat number, $L_v\kappa/K_L\Delta T_L$
t time
T temperature
T_M the freezing temperature of the pure substance
V velocity (u, v, w)
Z the non-dimensional surface deflection
x, y, z coordinates.

Greek symbols
α thermal expansion coefficient of the fluid density
γ surface tension
Γ capillarity constant
ΔT_L, ΔT_S the difference of temperature across the liquid layer and solid layer
η position of the solid–liquid interface
κ thermal diffusivity
Λ the non-dimensional solid–liquid interfacial deflection
μ viscosity of fluid
ν kinematic viscosity of fluid
ξ position of the upper free surface
ρ density of fluid
τ surface tension gradient with respect to temperature, $\partial\gamma/\partial T$
Ω_r, Ω_i real and imaginary growth rates with time.

Superscript
$'$ non-dimensional perturbed quantity.

Subscript
c critical value
i property of solid–liquid interface
L property of liquid layer
o initial value
r ratio of solid plate property to that of liquid
S property of solid plate.

$$V \times \vec{n}_i = 0, \tag{5a}$$

and the normal component satisifies:

$$\mathbf{v}_i \cdot \vec{n}_i(\rho_L - \rho_S) = (V \cdot \vec{n}_i)\rho_L, \tag{5b}$$

where $\mathbf{v}_i$ is the local solidification velocity, $\vec{n}_i$ is the unit vector normal to the solid–liquid interface, and ρ_L and ρ_S are the liquid and solid densities, respectively, at the solid–liquid interface. The conservation of energy at the solid–liquid interface satisfies:

$$(\mathbf{v}_i \cdot \vec{n}_t)L_v = (-K_L\nabla T + K_S\nabla T_S)\cdot\vec{n}_i, \tag{5c}$$

where L_v is the latent heat per unit volume and K_L and K_S are thermal conductivities of liquid and solid, respectively. With supercooling, the dependence of the freezing temperature on the capillary effect gives:

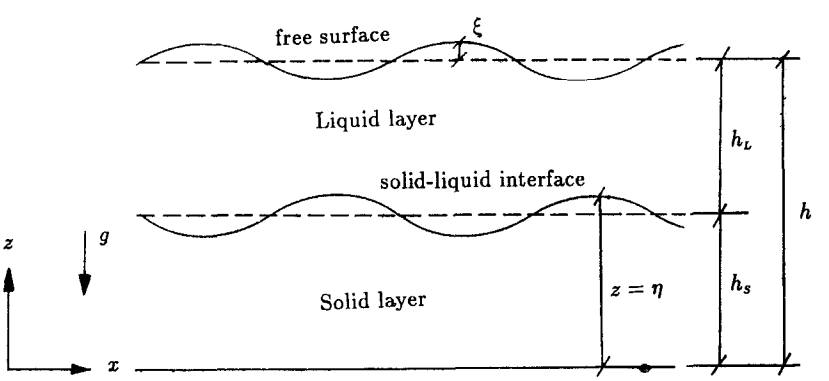

FIG. 1. Physical model.

$$T = T_S = T_i, \tag{5d}$$

$$T_i = T_M - T_M\Gamma\frac{\nabla_h^2\eta}{[1+(\nabla_h\eta)^2]^{3/2}}, \tag{5e}$$

where T_M is the freezing temperature of the pure substance, Γ is the capillarity constant, $\nabla_h^2 = \partial^2/\partial x^2 + \partial^2/\partial y^2$ is the horizontal Laplacian operator and $\nabla_h^2\eta/[1+(\nabla_h\eta)^2]^{3/2}$ is the mean curvature of the solid–liquid interface [1–7].

The governing equation for the temperature T_S in the solid layer is:

$$\frac{\partial T_S}{\partial t} = \kappa_S\nabla^2 T_S, \tag{6}$$

where κ_S is the thermal diffusivity coefficient of the solid layer. As usual, ∇^2 is the Laplacian operator:

$$\nabla^2 = \frac{\partial^2}{\partial x^2} + \frac{\partial^2}{\partial y^2} + \frac{\partial^2}{\partial z^2}. \tag{7}$$

The upper surface of the liquid layer is deformably free with its position at $z = h+\eta(x, y, t)$. The boundary conditions of velocity, heat flux and tangential and normal stresses at the free upper surface are [17]:

$$\frac{\partial\eta}{\partial t} + u\frac{\partial\eta}{\partial x} + v\frac{\partial\eta}{\partial y} = w \tag{8a}$$

$$K_L\nabla T\cdot\vec{n} + HT = 0 \tag{8b}$$

$$2\mu D_{nt} = \frac{\partial\gamma}{\partial T}\nabla T\cdot\vec{t} \tag{8c}$$

$$(p_a - p) + 2\mu D_{nn} = \gamma\nabla\cdot\vec{n}, \tag{8d}$$

where H is the heat transfer coefficient of the liquid layer, $\{D_{ij}\}$ is the rate of strain tensor in the fluid, $\vec{t}$ and $\vec{n}$ denote the tangential and the normal unit vectors at the free upper surface, and γ is the surface tension, for which we adopt the simple linear form:

$$\gamma = \gamma_0 - \tau(T - T_0), \tag{9}$$

where γ_0 is a constant reference value and τ is the rate of change with temperature. On the bottom face of the solid layer, the temperature T_S is kept fixed.

The basic solutions of steady-state consist of the zero velocity, the hydrostatic pressure p, the planar solid–liquid interface and the purely conductive temperature fields. After applying the boundary conditions to the energy equations, we get the basic linear temperature distributions in the liquid and solid layers

$$\bar{T} = T_i - \Delta T_L\frac{z-h_S}{h-h_S}, \tag{10a}$$

$$\bar{T}_S = T_i - \Delta T_S\frac{z-h_S}{h_S}, \tag{10b}$$

and

$$h = h_S + h_L. \tag{10c}$$

From the condition of energy conservation (5c) we have

$$A = \frac{h_S}{h_L} = \frac{K_S}{K_L}\frac{\Delta T_S}{\Delta T_L}. \tag{11}$$

Choosing h_L, h_L^2/κ, κ/h_L and ΔT_L as characteristic length, time, velocity and temperature, respectively, the perturbed governing equations of the liquid layer in the non-dimensional form can be obtained as:

$$\frac{1}{Pr}\frac{\partial}{\partial t}(\nabla^2 w') = R\nabla_h^2\theta' + \nabla^4 w', \tag{12}$$

$$\frac{\partial\theta'}{\partial t} = w' + \nabla^2\theta'. \tag{13}$$

Here w' and θ' are the non-dimensional z component of the perturbation velocity and temperature, respectively. Pr and R are the Prandtl number and Rayleigh number, defined as

$$Pr = \nu/\kappa \quad R = \alpha g\Delta T_L h_L^3/\nu\kappa. \tag{14}$$

The dimensionless perturbed governing equations of the solid layer are:

$$\frac{\partial\theta_S'}{\partial t} = \nabla^2\theta_S'. \tag{15}$$

Here the coordinates, time, and temperature are non-dimensionalized by h_S, h_S^2/κ_S and ΔT_S, respectively. θ_S is the non-dimensional z component of the perturbation temperature.

Similarly the dimensionless perturbed boundary conditions on the upper free surface at $z = h$ are:

$$\frac{\partial\xi'}{\partial t} = w', \tag{16a}$$

$$\frac{\partial\theta'}{\partial z} + Bi\,\theta' = Bi\,\xi', \tag{16b}$$

$$C\left[\frac{1}{Pr}\frac{\partial}{\partial t} + \left(\frac{\partial^2}{\partial z^2} + 3\nabla_h^2\right)\right]\frac{\partial w'}{\partial z} + (Bo - \nabla_h^2)\nabla_h^2\xi' = 0, \tag{16c}$$

$$\left(\frac{\partial^2}{\partial z^2} - \nabla_h^2\right)w' + M\nabla_h^2(\xi' - \theta') = 0, \tag{16d}$$

where ξ' is the non-dimensional surface deflection; C, Bi, Bo and M are the Crispation number, Biot number, Bond number and Marangoni number, defined as:

$$C = \mu\kappa/\gamma h_L \quad Bi = Hh_L/K_L$$

$$Bo = \rho g h_L^2/\gamma \quad M = \tau\Delta T_L h_L/\nu\kappa\rho. \tag{17}$$

The boundary conditions at the liquid–solid interface ($z = \eta$) are:

$$w' = \left(1 - \frac{\rho_S}{\rho_L}\right)\frac{\partial\eta'}{\partial t}, \tag{18a}$$

$$\frac{\partial w'}{\partial z} = 0, \tag{18b}$$

$$\theta' - \eta' = \frac{A}{K_r}(\theta_S' - \eta'), \tag{18c}$$

$$S\frac{\partial \eta'}{\partial t} = -\frac{\partial \theta'}{\partial z} + \frac{\partial \theta'_S}{\partial z}, \tag{18d}$$

$$\theta'_i - \eta' = C_a \nabla_h^2 \eta', \tag{18e}$$

where η' is the non-dimensional solid–liquid interface deflection; $K_r = K_S/K_L$ is the ratio of the thermal conductivities of solid layer to liquid layer; S and C_a are the latent heat number and the capillarity number, defined as:

$$S = L_v \kappa / K_L \Delta T_L \quad C_a = T_M \Gamma / \Delta T_L h_L. \tag{19}$$

The bottom boundary of the solid layer, at $z = 0$, is fixed with a constant temperature,

$$\theta'_S = 0. \tag{20}$$

The perturbation quantities in a normal mode form [1, 8] are:

$$(w', \theta', \eta', \xi') = [W(z), \Theta(z), \Lambda(z), Z(z)] \times \exp[i(a_x x + a_y y) + \Omega t], \tag{21a}$$

and

$$\theta'_S = \Theta_S(z_S) \exp[i(a_{Sx} x + a_{Sy} y) + \Omega t], \tag{21b}$$

where $a = \sqrt{a_x^2 + a_y^2}$ and $a_S = \sqrt{a_{Sx}^2 + a_{Sy}^2}$ are the wavenumber of the disturbances at the liquid and solid layers, respectively, and $a_S = Aa$, $z_L = (z - h_S)/h_L$ and $z_S = z/h_S$, $\Omega = \Omega_r + i\Omega_i$ is the reaction of the disturbances to the system, Ω_r is the growth rate. If $\Omega_r > 0$, the disturbances grow and the system becomes unstable, while, if $\Omega_r < 0$, the disturbances decay and the system becomes stable. When $\Omega_r = 0$, the instability of the system occurs in the marginal state, stationary ($\Omega_i = 0$) or oscillatory ($\Omega_i \neq 0$).

By substituting equations (21a) and (21b) into equations (12), (13) and (15), then the stationary governing equations of the perturbed state are:

$$(D^2 - a^2)^2 W = a^2 R\Theta, \tag{22}$$

$$(D^2 - a^2)\Theta = -W, \tag{23}$$

$$(D_S^2 - a_S^2)\Theta_S = 0, \tag{24}$$

where the operators $D = \partial/\partial z_L$ and $D_S = \partial/\partial z_S$.

The boundary conditions at the upper free surface, at $z = 1$, are:

$$W = 0, \tag{25a}$$

$$(D + Bi)\Theta = Bi\, Z, \tag{25b}$$

$$-C(D^2 - 3a^2)DW + (Bo + a^2)a^2 Z = 0, \tag{25c}$$

$$(D^2 + a^2)W + Ma^2(\Theta - Z) = 0. \tag{25d}$$

The boundary conditions at the solid–liquid interface, at $z = 0$ or $z_S = 1$, are:

$$W = 0, \tag{26a}$$

$$DW = 0, \tag{26b}$$

$$\Theta - \Lambda = \frac{A}{K_r}(\Theta_S - \Lambda), \tag{26c}$$

$$D\Theta = D_S \Theta_S, \tag{26d}$$

$$\Lambda = \frac{\Theta}{1 + C_a a^2}, \tag{26e}$$

and the boundary condition at the bottom surface, at $z_S = 0$, is:

$$\Theta_S = 0. \tag{27}$$

NUMERICAL PROCEDURE

The governing equations (22)–(24) and boundary conditions (25)–(27) form a Sturm–Liouville's problem with the Marangoni number M or Rayleigh number R being the eigenvalue and other physical parameters such as: C, Bo, Bi, A, K_r, C_a, a and a_S fixed. The shooting technique, based on the fourth-order Runge–Kutta–Gill's method [18], is used to solve the problem.

The first step in the procedure is to write equations (22) (24) as a system of first-order equations. Then we set, for the liquid layer:

$$W = u_1,$$

$$DW = Du_1 = u_2, \tag{28a}$$

$$D^2 W = Du_2 = u_3, \tag{28b}$$

$$D^3 W = Du_3 = u_4, \tag{28c}$$

$$\Theta = u_5,$$

$$D\Theta = Du_5 = u_6, \tag{28d}$$

$$D^4 W = Du_4 = 2a^2 u_3 - a^4 u_1 + Ra^2 u_5, \tag{28e}$$

$$D^2\Theta = Du_6 = a^2 u_5 - u_1, \tag{28f}$$

and, for the solid layer,

$$\Theta_S = v_1, \quad D_S\Theta_S = D_S v_1 = v_2, \tag{29a}$$

$$D_S^2\Theta_S = D_S v_2 = a_S^2 v_1. \tag{29b}$$

The shooting procedure starts from the upper boundary, at $z = 1$, and tries to match the boundary conditions at the liquid–solid interface, at $z = 0$ or $z_S = 1$, and then forward to match the boundary conditions at the lower boundary, at $z_S = 0$. The upper boundary conditions (25a)–(25d), at $z = 1$, can be expressed as:

$$u_1 = 0, \tag{30a}$$

$$u_3 = -3Ma^2 C/(Bo + a^2)u_2 + MC/(Bo + a^2)u_4 - Ma^2 u_5, \tag{30b}$$

$$u_6 = -3Bi\, C/(Bo + a^2)u_2 + Bi\, C/(Bo\, a^2 + a^4)u_4 - Bi\, u_5; \tag{30c}$$

we shall guess three boundary conditions:

$$u_2 = c_1 \quad u_4 = c_2 \quad u_3 = c_3, \tag{31}$$

then the general form of the solution becomes:

$$U = c_1 U_1 + c_2 U_2 + c_3 U_3, \tag{32}$$

where:

$$U = [u_1, u_2, u_3, u_4, u_5, u_6]^T, \tag{33a}$$

$$U_1 = [0, 1, -3Ma^2C/(Bo+a^2), 0, 0, -3BiC/(Bo+a^2)]^T, \tag{33b}$$

$$U_2 = [0, 0, MC/(Bo+a^2), 1, 0, BiC/(Bo\,a^2+a^4)]^T, \tag{33c}$$

$$U_3 = [0, 0, -Ma^2, 0, 1, -Bi]^T. \tag{33d}$$

We may guess a value for M or R, assume each of $U_{i,\,i=1,3}$ as a set of initial conditions and start the shooting procedure, using the Runge–Kutta–Gill's method of order four, from $z = 1$ and try to match the boundary conditions at the liquid–solid interface, at $z = 0$ or $z_S = 1$. The boundary conditions for $U_{i,\,i=1,3}$ at $z = 0$ are then transformed into a set of initial conditions for $V_{i,\,i=1,3}$ at $z_S = 1$, such that, using the boundary conditions (26c)–(26e):

$$V = c_1 V_1 + c_2 V_2 + c_3 V_3, \tag{34}$$

where

$$V = [v_1, v_2]^T, \tag{34a}$$

$$V_i^1 = \frac{K_r}{A} U_i^5 + \left(\frac{1}{A} - \frac{K_r}{A}\right)\frac{U_i^5}{(1+a^2C_a)}, \tag{34b}$$

$$V_i^2 = U_i^6, \tag{34c}$$

and the superscripts indicate the elements of U_i or V_i. Then, again, start using the same shooting procedure from $z_S = 1$ and try to match the boundary conditions at $z_S = 0$. The boundary conditions at the solid–liquid interface, (26c)–(26e), and at the lower boundary, (27), should be satisfied simultaneously and the results then turn into a matrix form,

$$\begin{pmatrix} U_1^1 & U_2^1 & U_3^1 \\ U_1^2 & U_2^2 & U_3^2 \\ V_1^1 & V_2^1 & V_3^1 \end{pmatrix} \begin{pmatrix} c_1 \\ c_2 \\ c_3 \end{pmatrix} = 0. \tag{35}$$

For c_i being non-trivial, the determinant of the matrix shall vanish. With fixed values of physical parameters A, K_r, C_a, C, Bi, Bo and wavenumbers a and a_S, the Rayleigh number R or Marangoni number M is thus solved with its critical value R_c or M_c marking the onset of instability at the marginal state.

RESULTS AND DISCUSSION

Validation

The numerical results are checked and compared with previous ones. Davis *et al.* [12] consider a fluid layer of single component with its both upper and lower boundaries rigid and isothermal (i.e. $Bi \to \infty$). The freezing process does occur from below and the solid–liquid interface is assumed flat (i.e. $C_a \to \infty$). The critical Rayleigh number as a function of the thickness ratio A is plotted in Fig. 2. The results are identical to those obtained by Davis *et al.* [12]. For the intermediate region of A, $0 < A < 1$, a strong dependence of the critical condition on the thickness ratio A is shown. It is of interest to note that R_c decreases with A monotonically, beginning at a value of 1707.818 and then approaching an asymptotic value of 1493.795.

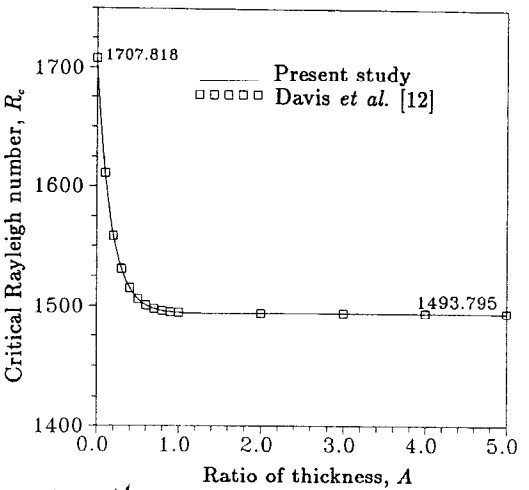

FIG. 2. The effect of A on the morphological instability with the Rayleigh–Bénard convection for $Bi \to \infty$, $C = 0$ and $C_a \to \infty$.

For the case $A = 0$, the system, before the freezing takes place, is treated as a layer of pure fluid with upper free and lower rigid boundaries. For the case $C = 0$ and $M = 0$, the system reduces to a classical Rayleigh–Bénard problem. An insulated upper surface (i.e. $Bi = 0$) gives rise to a critical condition $R_c = 669.234$ and $a_c = 2.086$, while an isothermal one (i.e. $Bi \to \infty$) does correspond to a critical condition $R_c = 1101.210$ and $a_c = 2.683$, as obtained by Sparrow *et al.* [10]. Similarly, in the absence of the thermal buoyancy (i.e. $R = 0$), we do recover a classical Marangoni problem with the critical condition $M_c = 79.603$ and $a_c = 1.993$ for $C = 0$ and $Bi = 0$, as previously obtained by Nield [15] and Carlos and Graciela [17].

Rayleigh–Bénard convection

The coupling mechanism between morphological and Rayleigh–Bénard convective instabilities (i.e. $M = 0$) is considered. Figure 3 presents the critical Rayleigh number R_c as a function of the thickness ratio A for various values of C_a. The thickness ratio A increases as the solidification proceeds. We find that the critical Rayleigh number R_c at a starting value 669.234 for $A = 0$ decreases sensitively with the thickness ratio A for $0 < A < 1$ and then approaches a fixed value for large values of A. It indicates that the growth and deformation of the solid–liquid interface results in a sequence of perturbations of thermal convection, which in turn affect the interfacial movement. The capillary effect of the solid–liquid interface does

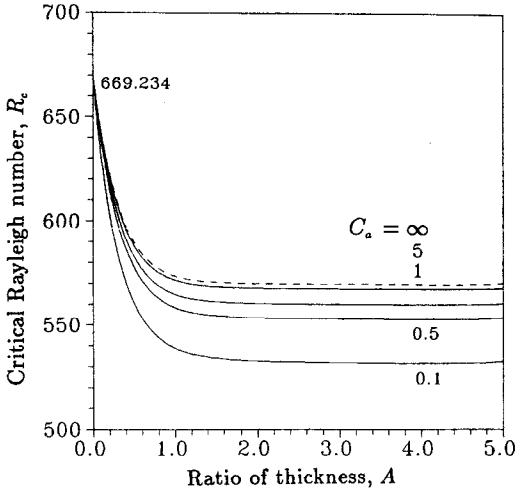

FIG. 3. The effect of C_a and A on the morphological instability with the Rayleigh–Bénard convection for $K_r = 2$, $Bi = 0$ and $M = 0$.

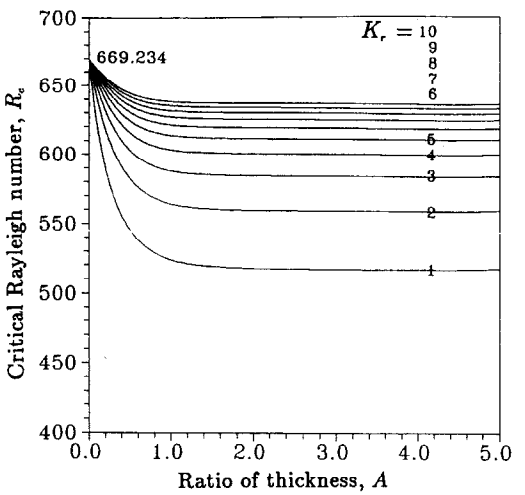

FIG. 4. The effect of K_r and A on the morphological instability with the Rayleigh–Bénard convection for $C_a = 1$, $Bi = 0$ and $M = 0$.

suppress the interfacial growth and deformation acts as the stabilizing factor for the thermally convective instability. The critical Rayleigh number R_c increases as the capillarity number C_a increases. The dashed curve in Fig. 3 corresponds to a limiting case (i.e. $C_0 \to \infty$), when the solid–liquid interface is planar.

The latent heat, released at the solid–liquid interface during the solidification, is conducted away from above or below and has a dominant effect on either the thermally convective or the morphological instability. As shown in Fig. 4, the critical Rayleigh number R_c increases as the ratio of thermal conductivities K_r increases. Physically, the more the latent heat is conducted away through the solid layer and the less it is stored in the liquid layer the more the system will become stable. The influence of the heat transfer at the free upper surface on the system is shown in Table 1 and Fig. 5. When the upper surface is perfectly insulated (i.e. $Bi = 0$), any thermal disturbance can not easily dissipate into the ambience and hence the system becomes more destabilizing and has a smaller critical value. The dashed curve corresponds to the critical values, when the Biot number Bi approaches infinity (i.e. $Bi \to \infty$), at which the upper surface is isothermally and perfectly conducting. The critical Rayleigh number R_c increases with the Biot number Bi.

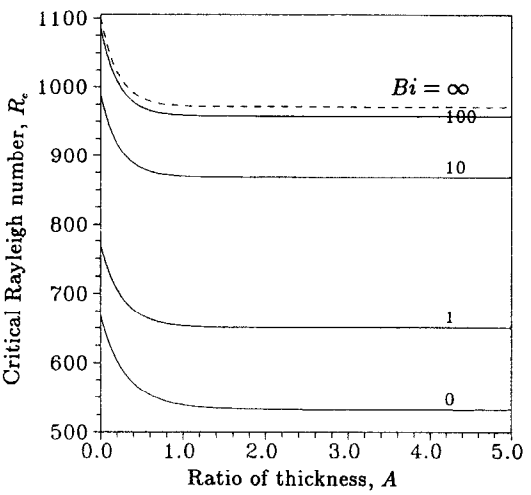

FIG. 5. The effect of Bi and A on the morphological instability with the Rayleigh–Bénard convection for $K_r = 2$, $C_a = 0.1$ and $M = 0$.

Table 1. Critical values of Rayleigh number R_c and the corresponding critical wavenumber a_c for different values of Bi and A on the morphological instability with the Rayleigh–Bénard convection ($K_r = 2$, $C_a = 0.1$ and $M = 0$)

	$A = 0$				$A = 0.1$		$A = 0.5$		$A = 1$		$A = 2$	
	Sparrow *et al.* [10]		Present study									
Bi	R_c	a_c	R_c	a_c	R_c	a_c	R_c	a_c	R_c	a_c	R_c	a_c
0	669.001	2.09	669.234	2.086	630.074	2.001	560.416	1.776	538.779	1.643	532.747	1.576
1	770.569	2.3	770.860	2.293	731.832	2.223	668.477	2.053	653.600	1.975	651.029	1.952
10^1	989.493	2.59	989.947	2.589	945.870	2.527	881.242	2.387	869.905	2.338	868.640	2.328
10^2	1085.893	2.67	1086.450	2.672	1038.680	2.610	970.488	2.472	959.352	2.427	958.228	2.419
10^3	1100.657	2.68	1099.690	2.682	1051.354	2.619	982.567	2.482	971.423	2.436	970.311	2.429
∞	1101.650	2.68	1101.210	2.683	1052.814	2.621	983.957	2.483	972.811	2.438	971.701	2.430

Table 2. Critical values of Marangoni number M_c and the corresponding critical wavenumber a_c for different values of C and A on the morphological instability with the Marangoni convection ($Bo = 0.1$, $Bi = 0$, $K_r = 2$, $C_a = 0.1$ and $R = 0$)

	$A = 0$											
	Carlos [17]		Present study		$A = 0.1$		$A = 0.5$		$A = 1$		$A = 2$	
C	M_c	a_c	M_c	a_c	M_c	a_c	M_c	a_c	M_c	a_c	M_c	a_c
0	79.607	1.99	79.603	1.993	77.125	1.928	72.187	1.757	70.532	1.663	70.092	1.622
10^{-6}	79.606	1.99	79.602	1.993	77.124	1.928	72.186	1.757	70.531	1.663	70.090	1.622
10^{-5}	79.596	1.99	79.593	1.993	77.113	1.927	72.174	1.757	70.517	1.663	70.075	1.621
10^{-4}	79.499	1.99	79.496	1.989	77.011	1.923	72.053	1.751	70.381	1.656	69.930	1.613
10^{-3}	66.667	0.00	66.667	0.001	66.667	0.001	66.667	0.00	66.667	0.001	66.667	0.001
10^{-2}	6.667	0.00	6.667	0.001	6.667	0.001	6.667	0.00	6.667	0.001	6.667	0.001
10^{-1}	0.667	0.00	0.667	0.001	0.667	0.001	0.667	0.00	0.667	0.001	0.667	0.001

Marangoni convection

In the absence of the thermal buoyancy (i.e. $R = 0$), the coupling effects of the morphological and Marangoni convective instabilities are considered. The morphological effects include the thickness and thermal conductivity of the solid and the capillary effect of the solid–liquid interface. Before the system starts freezing (i.e. $A = 0$), the critical Marangoni number M_c, for various values of the Crispation number C, are tabulated in part of Table 2, previously obtained by Carlos and Graciela [17]. The Crispation number C, associated with the inverse effect of the surface tension, shows the rigidity of the free upper surface of the liquid layer. From Table 2 and Fig. 6, the critical Marangoni number M_c decreases as the Crispation number C increases. These decreasing trends are negligible for $0 \leqslant C \leqslant 10^{-4}$, in which ranges the values of the critical wavenumbers are finite and approximately fixed, while the same decreasing trends become proportional and significant for $C \geqslant 10^{-3}$, in which ranges the values of the critical wavenumbers are vanishing. There exists a Crispation number C in the range 10^{-4}–10^{-3} such that a jump on the Marangoni convective instability from a finite critical wavenumber to a vanishing one does exist. For each value of the Crispation number C, there are, on the neutral curve, two minimal points with either finite or vanishing wavenumber a, corresponding to two different and possible modes of Marangoni convective instabilities, one of which, with the smaller value of the Marangoni number, being the critical one, would occur in the marginal state, as shown in Fig. 7a and b.

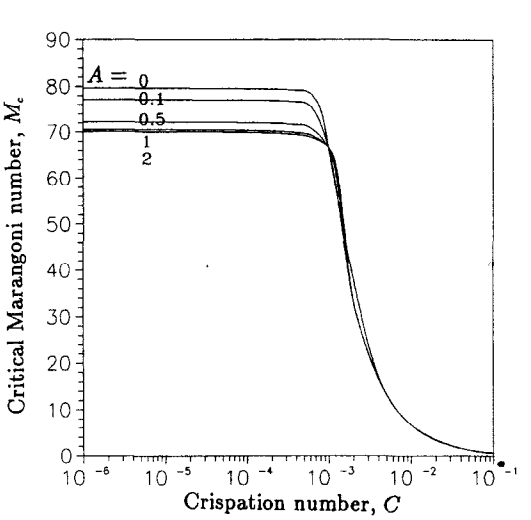

FIG. 6. The effect of C and A on the morphological instability with the Marangoni convection for $K_r = 2$, $C_a = 0.1$, $Bo = 0.1$, $R = 0$ and $Bi = 0$ at the upper surface.

For the whole range of the Crispation number, the critical Marangoni number M_c, as before, decreases as the thickness ratio A increases and it increases as the capillarity number C_a increases.

The Marangoni number M, corresponding to the first minimal point of zero wavenumber, is very indifferent to effects of both the thickness ratio A and the capillarity number C_a, but it is quite sensitive to the surface tension of the free upper surface, while that corresponding to the second minimal point of finite wavenumber decreases with the thickness ratio A and increases with the capillarity number C_a sensitively.

The Bond number Bo of the upper free surface, being a ratio of the gravity effect to the effect of surface tension, indicates the dominant one of the two effects in flattening a curved free surface. Here, we take the Bond number $Bo = 0.1$ for simplicity.

As shown in Fig. 8, the critical Marangoni number M_c increases as the ratio of thermal conductivities K_r increases. Physically, the more the latent heat is conducted from below through the solid layer, the less it is stored in the liquid layer such that the thermal disturbances are weaker at the upper free surface: therefore, the system becomes more stabilizing.

Bénard–Marangoni convection

The coupling effects of Bénard–Marangoni convective and morphological instabilities are considered. The values of some physical parameters are chosen as $K_r = 2$, $C_a = 0.1$ and $C \leqslant 10^{-3}$. The critical Rayleigh number R_c as a function of the thickness ratio A, for fixed positive values of the Marangoni number M, is shown in Fig. 9. An increment in the Marangoni number, as a result of a larger variation of the surface tension with the temperature, indicates a decrement in the surface tension. We predict that the critical

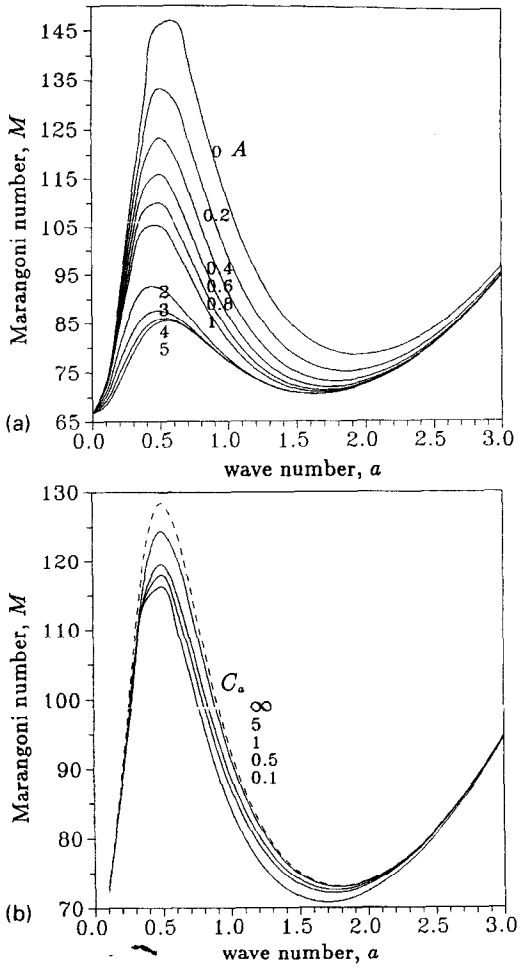

FIG. 7. (a) The stationary neutral curves $M(a)$ are plotted for several values of A on the morphological instability with the Marangoni convection for $C = 10^{-3}$, $K_r = 2$, $C_a = 1$, $Bo = 0.1$, $Bi = 0$ and $R = 0$. (b) The stationary neutral curves $M(a)$ are plotted for several values of C_a on the morphological instability with the Marangoni convection for $C = 10^{-3}$, $A = 0.5$, $K_r = 2$, $Bo = 0.1$, $Bi = 0$ and $R = 0$.

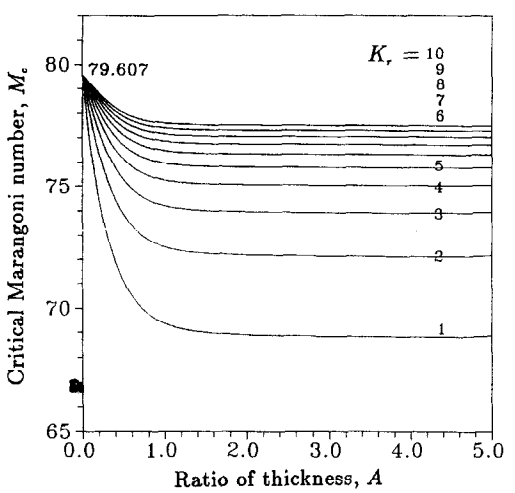

FIG. 8. The effect of K_r and A on the morphological instability with the Marangoni convection for $C_a = 1$, $C < 10^{-3}$, $Bo = 0.1$, $Bi = 0$ and $R = 0$.

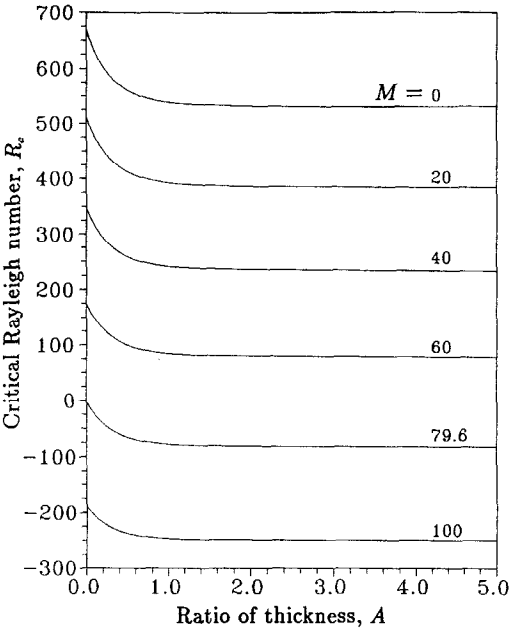

FIG. 9. The effect of M and A on the morphological instability with the Bénard–Marangoni convection for $C < 10^{-3}$, $K_r = 2$, $C_a = 0.1$, $Bo = 0.1$ and $Bi = 0$ at upper surface.

Rayleigh number R_c decreases as the Marangoni number M increases. For $M \geqslant 79.603$, the critical Rayleigh number R_c becomes negative and the Marangoni convective instability is solely dominant. The locus of (M_c, R_c) at the marginal state, for various values of A and $Bi = 0$, is plotted in Fig. 10. When the Marangoni number $M = 0$ and the thickness ratio $A = 0$, corresponding to the dashed curve, the critical Rayleigh number R_c is 669.234 and decreases as the value of the thickness ratio A increases and approaches a limiting value of 532.446. Similarly, the same dashed curve, for the Rayleigh number $R = 0$ and $A = 0$, gives the critical Marangoni number $M = 79.603$ and it decreases as the thickness ratio A increases and approaches a limiting value of 70.072. The results indicate that the increments of the Rayleigh number, Marangoni number and thickness ratio A tend to destabilize the system.

CONCLUSIONS

The linear and stationary analysis of the critical conditions for the coupling effects of the Bénard–Marangoni convective and morphological instabilities of a horizontal liquid layer of a single component during the solidification has been studied. The following results have been obtained.

1. The morphological effects, including the thickness and thermal conductivity of solid layer and the capillary effect of the solid–liquid interface have significant influences on the onset of instability at the marginal state. A larger value of the capillary

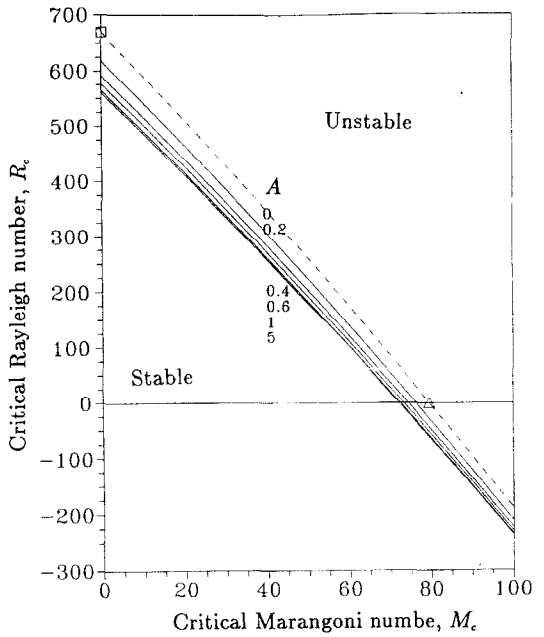

FIG. 10. Locus of critical Marangoni number M_c and critical Rayleigh number R_c for different values of A in $C < 10^{-3}$, $K_r = 2$, $C_a = 0.1$, $Bo = 0.1$ and $Bi = 0$ at upper surface: □— $R_c = 669.234$; △- - $M_c = 79.603$).

effect and thermal conductivity in the solid layer tends to stabilize the system.

2. The critical conditions, R_c and M_c, decrease sensitively as the thickness ratio A increases for $0 < A < 1$ and approach fixed values.
3. The conduction of the latent heat has a dominant role in determining the possible stability of the system. Similarly, as the Biot number Bi, associated with the conductive character of the heat transfer at the upper free surface, increases, the system become more stabilizing.

REFERENCES

1. R. F. Sekerka, Morphological stability. In *Crystal Growth: An Introduction* (Edited by P. Hartman), pp. 403–443. North-Holland (1973).
2. S. R. Coriell, M. R. Cordes and R. F. Sekerka, Convective and interfacial instability during unidirectional solidification of a binary alloy, *J. Crystal Growth* **49**, 13 28 (1980).
3. W. W. Mullins and R. F. Sekerka, Stability of a planar interface during solidification of a dilute binary alloy, *J. Appl. Physics* **35**, 444–451 (1964).
4. S. R. Coriell and R. F. Sekerka, Effect of convection flow on morphological stability, *PhysicoChemical Hydrodynamics* **2**, 281 293 (1981).
5. D. T. J. Hurle, E. Jakeman and A. A. Wheeler, Effect of solutal convection on the morphological stability of a binary alloy, *J. Crystal Growth* **58**, 163–179 (1980).
6. D. T. J. Hurle, E. Jakeman and A. A. Wheeler, Hydrodynamic stability of the melt during solidification of a binary alloy, *Phys. Fluids* **23**, 624–627 (1983).
7. L. S. Langer, Instabilities and pattern formation in crystal growth, *Rev. Mod. Phys.* **52**, 1 28 (1980).
8. R. Ananth and W. N. Gill, Dendritic growth with thermal convection, *J. Crystal Growth* **91**, 587 598 (1988).
9. K. Brattkus and S. H. Davis, Flow induced morphological instabilities: stagnation-point flows, *J. Crystal Growth* **89**, 423–427 (1988).
10. E. M. Sparrow, R. J. Goldstein and V. K. Jonsson, Thermal instability in a horizontal fluid layer: effect of boundary conditions and non-linear temperature, *J. Fluid Mech.* **18**, 513–529 (1964).
11. D. A. Nield, The thermohaline Rayleigh–Jeffreys problem, *J. Fluid Mech.* **29**, 545–558 (1967).
12. S. H. Davis, U. Muller and C. Dietsche, Pattern selection in single-component systems coupling Bénard convection and solidification, *J. Fluid Mech.* **144**, 133–151 (1984).
13. J. R. A. Pearson, On convection cell induced by surface tension, *J. Fluid Mech.* **4**, 489–500 (1958).
14. L. E. Scriven and C. V. Sternling, On cellular convection driven by surface tension gradients: effect of mean surface tension and surface viscosity, *J. Fluid Mech.* **19**, 321–340 (1965).
15. D. A. Nield, Surface tension and buoyancy effect in cellular convection, *J. Fluid Mech.* **19**, 341 352 (1965).
16. S. H. Davis and G. M. Homsy, Energy stability theory for free-surface problem: buoyancy-thermocapillary layers, *J. Fluid Mech.* **98**, 527–553 (1980).
17. P. G. Carlos and C. Graciela, Linear stability ananlysis of Bénard–Marangoni convection in fluids with a deformable free surface, *Phys. Fluids A* **3**, 292–298 (1991).
18. A. Davey, *Numerical Methods for the Solution of Linear Differential Eigenvalue Problem*, pp. 485–498. University of Newcastle Upon Tyne Press (1976).